Electrochemical Studies on a Thin Film of Nickel Sulphide Prepared by SILAR Method

N. Karthika[1], B. Gomathi[1], A. L. Jewelcy[1], P. S. L. Kala[1], A C. Jamuna[1], R. Jeyalakshmi[1], M. Pushpa[1], N. Anitha[1] and S. Rajendran[1,2*]

[1]Corrosion Research Centre, Department of Chemistry, St Antony's College of Arts and Sciences for Women (Affiliated to Mother Teresa Women's University, Kodaikanal), Dindigul, Tamil Nadu, India

[2] Centre for Nanoscience and Technology, Pondicherry University, Puducherry, India

*Corresponding author: susairajendran@gmail.com

Received 03/02/2024; accepted 30/04/2024
https://doi.org/10.4152/pea.2026440105

Abstract

In the present study, a thin film of Ni_xS_y was deposited on an ITO GP by SILAR method. This film was characterized by UV-vis reflectance and FTIR spectroscopy. UV-vis reflectance revealed that E_g from Ni_xS_y was 1.55 eV. After coating, ITO GP E_g decreased from 1.88 to 1.55 eV. This indicates that the film functioned as a semi conductor. UV-vis absorbance showed that the film absorbance occurred at 322.00, 388.80 and 396.25 nm, with peak intensity of 1.229, 0.934 and 0.916 AU, respectively. FTIR spectra confirmed Ni_xS_y formation on ITO GP by SILAR technique. Thus, it was encouraging to note that Ni_xS_y was successfully prepared by this method. Electrochemical studies, such as polarization technique and AC impedance spectra revealed that current flowing through ITO GP increased after Ni_xS_y coating by SILAR method. These findings may be useful for solar panel systems used in marine environments.

Keywords: E_g; electrochemical studies; ITO GP; Ni_xS_y; SILAR method; thin film.

Introduction•

Thin film materials have been used in semiconductor devices, wireless communications, telecommunications, integrated circuits, rectifiers, transistors, solar cells, light emitting diodes, photoconductors, light crystal displays, lithography, micro-electromechanical systems, multifunctional emerging coatings and other emerging cutting technologies. SILAR is one of the chemical methods for creating uniform and large area thin films, which is based on the substrate immersion into separate cations and anions. Compared to other methods, SILAR is a simple, economic and less time-consuming method for binary semiconducting thin films

•The abbreviations and symbols definition lists are in page 81.

deposition. It is also applicable for the deposition of large-area thin films. Several research papers on SILAR methods have been published [1-10].

ZnO, CdO and CdZnO thin films deposited by chemical routes such as spray pyrolysis, sol-gel spin coating, SILAR, deposition by electricity, baths, chemical vapor, atomic layer and pulsed vapor have been discussed by [1].

CO_2 photoconversion to solar fuels requires materials with a high affinity to the acidic CO_2, and MgO and $Mg(OH)_2$ films represent good candidates, since their basic sites are highly active for CO_2 capture in a wide interval of temperatures. However, MgO and $Mg(OH)_2$ deposition as thin films is difficult to obtain by traditional methods. As an alternative, SILAR method was proposed by [2], to obtain $MgO/Mg(OH)_2$ mixtures over glass substrates, at lower temperatures from 200 to 400 °C. The films were tested as photocatalysts in CO_2 photoconversion to solar fuels (HCOOH and CH_3OH) under UV-vis near infrared irradiation.

[3] have designed a reactor to coat a PbS thin film on glass substrate by continuous flow. A methodology has been proposed to deposit PbS films based on reducing the roughness via a laminar and continuous flow in the reactor, of which turbulent properties are hindered. The modified coating method was named FTCD. Morphological analysis has demonstrated that the surface roughness of PbS films deposited by FTCD method was lower than that of the other films.

[4] have investigated ZnS nanolayer over Co doped ZnS-CdS–TiO_2 nanocomposite thin films on glass substrates by bottom-up approaching methods. This nanolayer protects CdS nanocrystal, which enhances photo stability. Structural, optical, electrical and surface morphological properties of ZnS–Co CdS–TiO_2 composite thin films have been systematically evaluated. Structural analysis has indicated that Co^{2+} have been successfully incorporated into CdS site. Co doping into ZnS–CdS–TiO_2 film increased the lattice parameter. E_g decreased with higher Co concentrations, indicating the easy path for electron transfer from valences to the film conduction band.

To create new flexible TE and photosensitive thin-film material for in-plane TE generator and broadband photodetector, [5] have deposited nanostructured ZnO:In doped thin films on polyimide substrates by using inexpensive and scalable SILAR method. To reduce ZnO:In film resistivity in ZnO:In/PI composition to about 0.02 Ω/m, it was annealed in a vacuum, at 300 °C.

[6] have firstly reported controlled growth of pseudocapacitive nanostructured Ag_2Se thin films, through simple, less expensive, room temperature and industry scalable SILAR method onto stainless steel substrate, to be used as electrode material for supercapacitor applications. X-ray photoelectron spectroscopy studies confirmed Ag_2Se formation. Orthorhombic structure of grown Ag_2Se thin film had hydrophilic nature in aqueous Na_2SO_3 electrolyte, yielding specific capacitance of 112.45 F/g and 10 mV/s scan rate studied through cyclic voltammetry.

[7] have reported the effects of different H_2O_2 concentrations on the growth velocity of ZnO thin films deposited by SILAR method. H_2O_2 effects on the films' growth velocity have been studied by RBS technique. Results have shown an increase in

thickness from 0 to 290 ± 20 [nm], with higher H_2O_2 concentrations from 0 to 30%, which has evidenced its strong catalyzer effect on the films' growth velocity.

Since B_i2S_3 has attracted much interest as a semiconductor material for solar cell applications, [8] have reported the synthesis of its thin films through an economical and simply modified SILAR method, with the use of 2-methoxyethanol as complexing agent, and with post-annealing of the thin films at 200 °C, under inert Ar-atmosphere. The influence of SILAR cycles number (30, 40 and 50) on structural, morphological and optical properties of the synthesized B_i2S_3 thin films onto a glass substrate has been investigated. The samples have been characterized by techniques such as X-ray diffraction, Energy-Dispersive X-ray and Raman spectroscopy, Scanning Electron Microscopy and UV-vis spectrophotometry.

[9] have investigated the growth of a low temperature solution by SILAR, for deposition of nanostructured ZnO and ZnO:In doped thin films on flexible polyimide substrates, for use as cheap non-toxic TE materials in flexible modules of planar type, to power up portable electronics and miniature devices. By SILAR method, a zincate solution has produced a ZnO:In film which, after post-growth annealing at 300 °C, had low resistivity of $\rho \approx 0.02\ \Omega$ m, high Seebeck coefficient of 147 μV/K and TE power factor of ~1 $\mu W/K^{-2}/m^{-1}$, at near-room temperatures. To attest the operability of manufactured films as the basis of TE devices, the study designed and tested an experimental lightweight thin-film TE module, which was able to produce specific output power of 0.8 $\mu W/m^2$, at 50 K.

The use of free-standing sulfide-based hybrid nanostructures plays a paramount role in supplying the steadily increasing demand for energy storage devices. [10] have reported the growth of outstanding binder-free Ni-Sn sulfide thin films for high-performance supercapacitors via revised SILAR method. Molar concentration ratios for Ni/Sn have been studied, and the optimum designed mesoporous Ni_x-Sn 1.0 x S/Ni foam, a single cathode electrode material, successfully achieved outstanding specific capacitance of 2890 F/g, at 5 A/g, capacitance retention of 85%, and coulombic efficiency of 100% after 10,000 cycles. Moreover, the constructed activated carbon hybrid supercapacitor device delivered an ultrahigh power density of 53.469 kW/Kg and capacitance retention of 95%, with robust long-term cycling stability up to 1000 cycles.

[11] have employed SILAR to investigate deposited Cu_2MnSnS_4 thin films for sustainable energy applications. [12] have performed facile synthesis of layered reduced graphene oxide/polyaniline composite electrode for a flexible asymmetric solid-state supercapacitor. [13] have investigated the synthesis, microstructural and optoelectronic properties of Cd-supported CuO-ZnO binary oxide thin films.

[14] have carried out facile synthesis and characterization of TiO_2/SnS nanocomposites by eco-friendly methods. [15] have researched the effect of SILAR cycle on In_2O_3 thin films gas sensing properties for CO gas sensor.

In the present work, a Ni_xS_y thin film on ITO GP was prepared by SILAR method. The thin film was characterized by Uv-vis reflectance and FTIR spectra. Electrochemical studies on the thin film were carried out by polarization and AC impedance spectra.

Materials and methods

In the present study, Ni_xS_y thin film coated ITO GP was prepared by SILAR method, by its successive dipping in distilled water, sodium sulphide, distilled water and nickel sulphate solutions (Fig. 1).

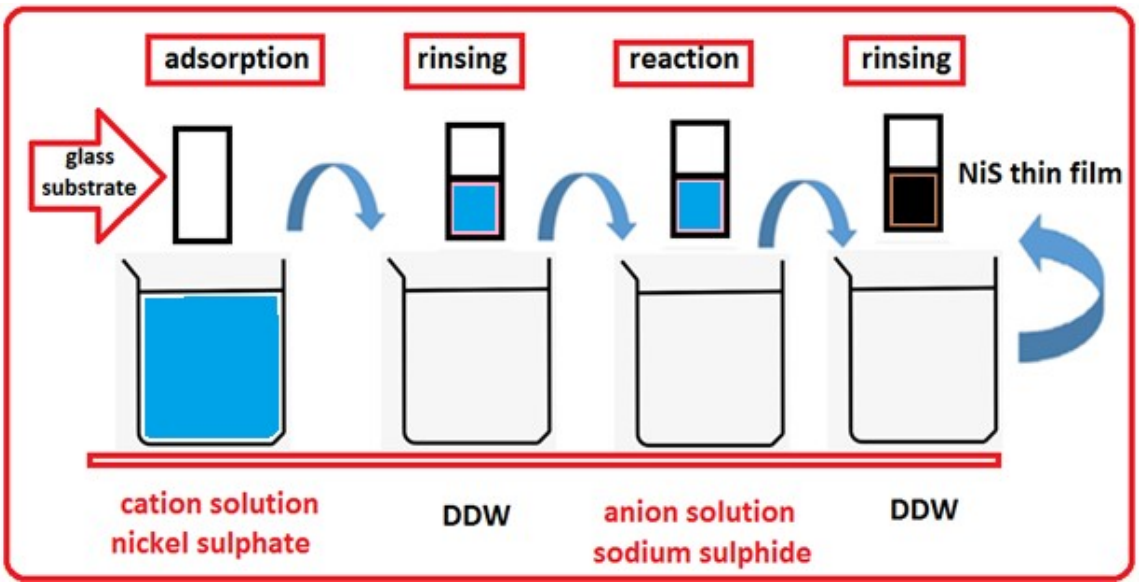

Figure 1: Ni_xS_y thin film on ITO GP prepared by SILAR method.

UV-vis spectroscopy

UV-vis spectra were recorded in Agilent diode array spectrometer (Agilent 8453).

FTIR spectroscopy

FTIR spectra were recorded in a Perkin Elmer 1600 series model, with resolving power of 4 cm^{-1}.

Electrochemical studies

The corrosion resistance of Ni_xS_y thin film coated on ITO GP prepared by SILAR method, without and with SW, was evaluated by electrochemical studies such as polarization technique and AC impedance spectra.

Polarization study

A 660A model CHI electrochemical work station with impedance was used for this purpose. A three-electrode cell assembly electrode was employed. ITO GP before and after coating, SCE and Pt were used as working reference and counter electrodes, respectively. From the polarization study, corrosion parameters, such as E_{corr}, I_{corr}, β_a, β_c and LPR were calculated. Scan rate (V/S) was 0.01. Hold time at E_{fcs} was 0, and quit time (sec) was 2. Tafel slope potential range was 0.06 V, as a built-in arrangement.

AC impedance spectra

AC impedance spectral studies were carried out on a Model 660A CHI electrochemical workstation. SCE and Pt were used as reference and counter electrodes, respectively. The real (Z') and imaginary (-Z'') parts of the cell impedance were measured in ohms, at various frequencies. R_{ct}, C_{dl}, impedance and phase angle values were calculated from Nyquist and Bode plots. The frequency range was selected depending on open circuit potential.

Results and discussion

Analysis of UV-vis spectra

UV-vis spectra (absorbance and transmittance) of ITO GP before and after coating with Ni_xS_y by SILAR method are shown in Figs. 2-5. UV-vis (Fig. 2) shows that ITO GP absorbance took place at 324.50 and 521.75 nm, with peak intensity of 0.062 and 0.061 (AU), respectively.

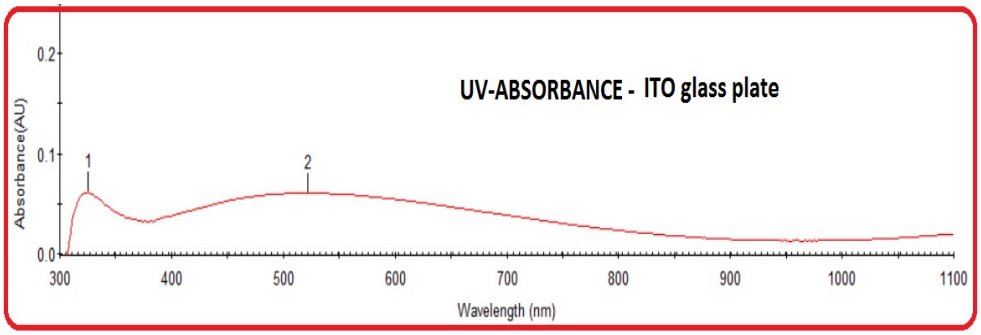

Figure 2: UV-vis absorbance spectrum of ITO GP.

UV-vis spectrum of ITO GP after coating with Ni_xS_y by SILAR method (Fig. 3) shows that absorbance took place at 322.00, 388.80 and 396.25 nm, with peak intensity of 1.229, 0.934 and 0.916 (AU), respectively.

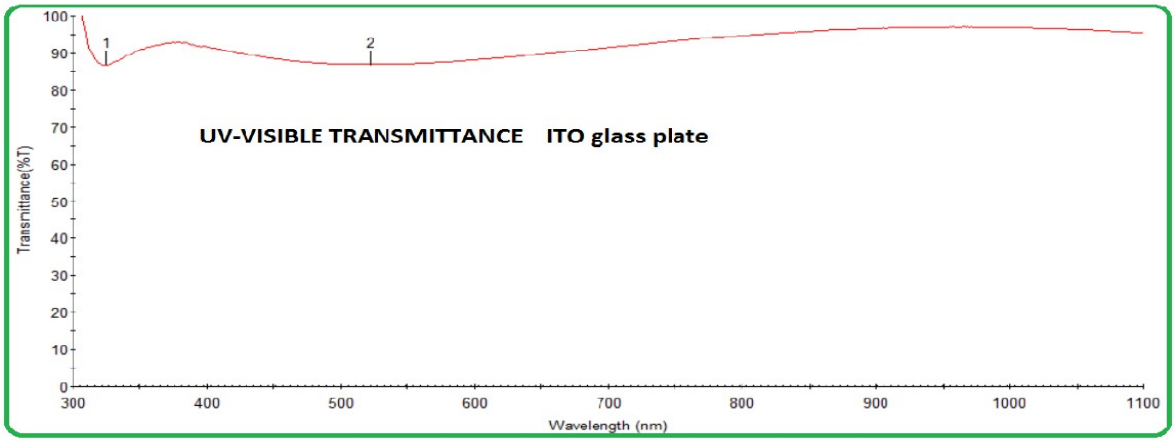

Figure 3: UV-vis transmittance spectrum of ITO GP.

The new peaks were due to Ni_xS_y on the ITO GP. The increase in intensity indicates that the electrons jumped freely and easily onto Ni_xS_y. E_g from coated ITO GP was lower than that without coating. UV-vis spectrum of ITO GP (Fig. 4) shows that wavelength transition took place at 660 nm. So, E_g = 1.239/0.660 = 1.88 eV.

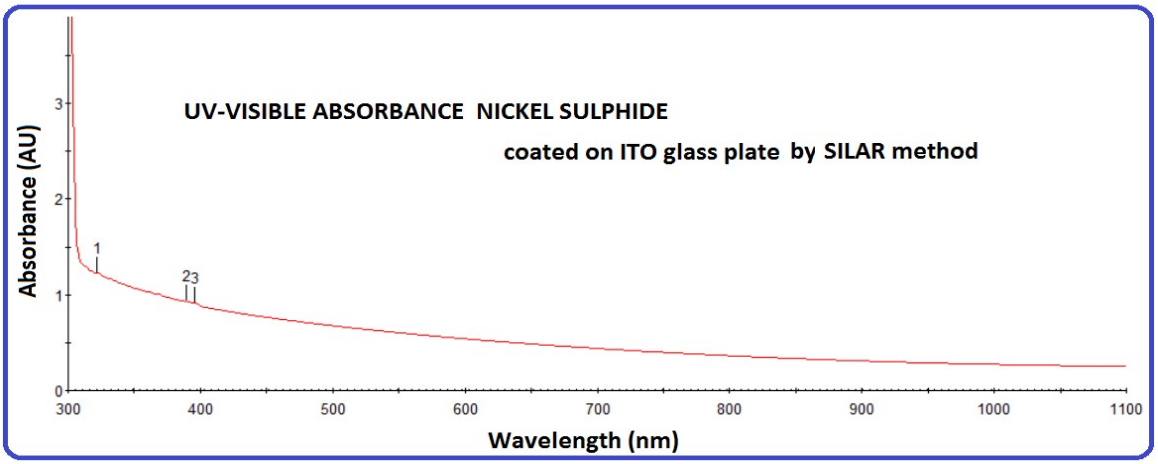

Figure 4: UV-vis absorbance spectrum of ITO GP coated with Ni_xS_y by SILAR method.

UV-vis transmittance spectrum of coated ITO GP (Fig. 5) reveals that wavelength transition took place at 800 nm. So, E_g = 1.239/0.800 = 1.55 eV. It is interesting to note that, after ITO GP coating, its E_g decreased. So, electron flow was enhanced. This finding will be useful for solar cells.

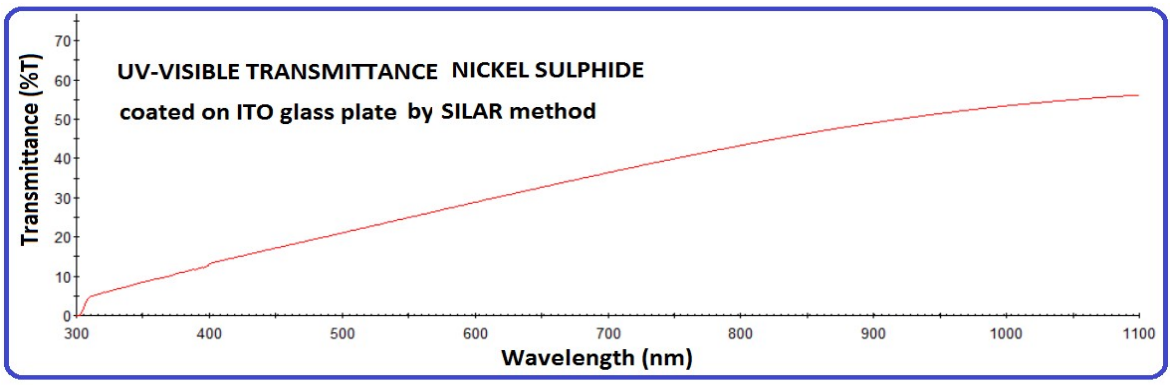

Figure 5: UV-vis transmittance spectrum of ITO GP coated with Ni_xS_y by SILAR method.

Analysis of FTIR spectra

FTIR spectrum (KBr) of Ni_xS_y thin film coated on ITO GP by SILAR method is shown in Fig. 6(a-c).

Peaks at 514 and 2926 cm^{-1} confirm the presence of Ni_xS_y on ITO GP [11, 16].

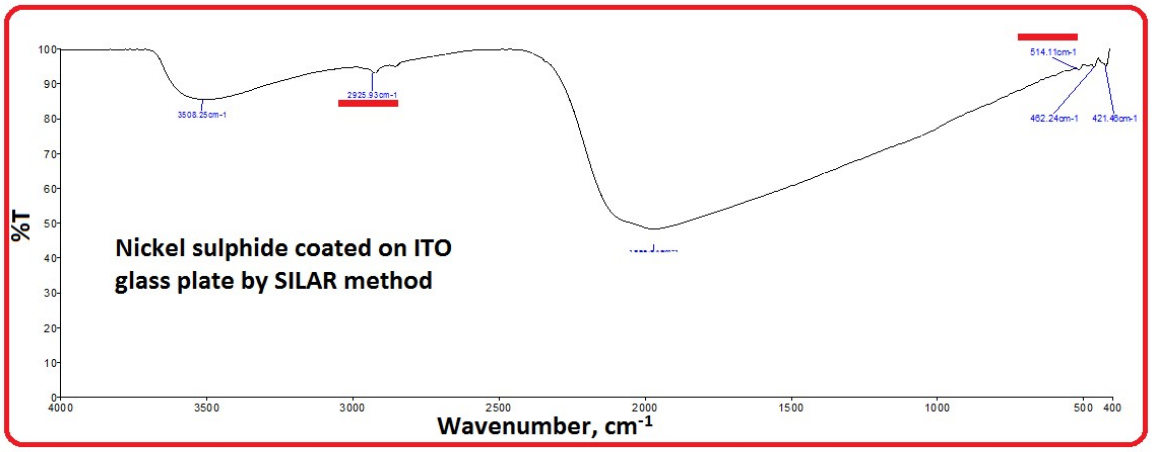

(a)

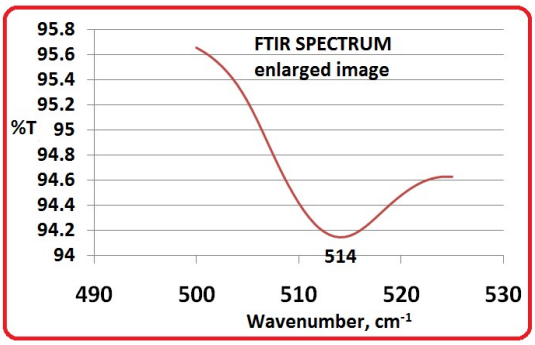

(b)

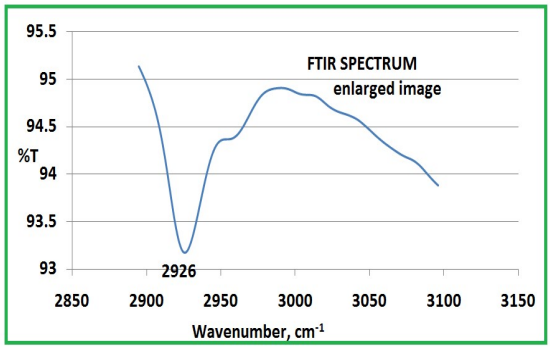

(c)

Figure 6: FTIR spectra of- **(a)** (KBr) of Ni_xS_y thin film coated on ITO GP by SILAR method**;** enlarged image of peak at- **b)** 514 cm^{-1}; **(c)** 2926 cm^{-1}.

Polarization study

Polarization curves of ITO GP immersed in SW before coating and after coating (with Ni_xS_y) are shown in Fig. 7.

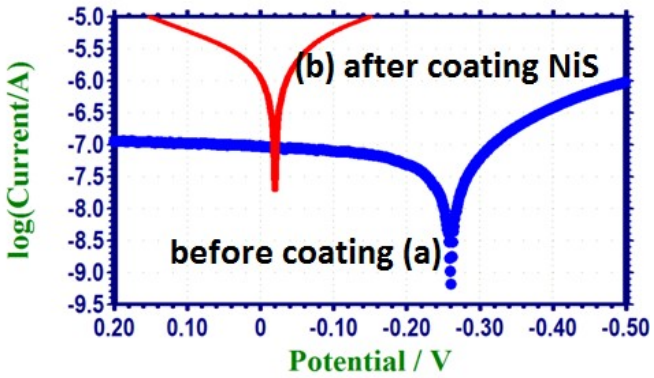

Figure 7: Polarization curves of ITO GP immersed in SW- before **(a)**; and after **(b)** coating with Ni_xS_y.

Polarization parameters, namely, E_{corr}, β_c, β_a, LPR and I_{corr} are given in Table 1.

Table 1: Corrosion parameters obtained from polarization study of ITO GP in SW before and after Ni_xS_y coating by SILAR method.

System	E_{corr} mV/vs SCE	β_c mV/dec	β_a mV/dec	LPR Ohm/cm^2	I_{corr} A/cm^2
Uncoated ITO GP in SW	-261	136	494	889526	5.221×10^{-8}
Ni_xS_y coated ITO GP in SW	-20	185	257	16796	278.1×10^{-8}

Table 1 shows that, when ITO GP was immersed in SW, E_{corr} was -261 mV *vs.* SCE. I_{corr} flowing through the system was 5.221 x 10^{-8} A/cm^2. LPR value was 889526 Ohm/cm^2. When Ni_xS_y film coated ITO GP was immersed in SW, E_{corr} shifted to the anodic side (-20 mV *vs.* SCE). LPR value decreased from 889526 to 16796 Ohm/cm^2. I_{corr} flowing through the system increased from 5.221 × 10^{-8} to 278.1 × 10^{-8} A/cm^2. Thus, it is inferred that, with films coatings, the current flowing through the system increases in marine environments [17-21]. So, such GP can be used in solar panels in marine environments.

Analysis of AC impedance spectra

AC impedance spectra of ITO GP immersed in SW before and after coating with Ni_xS_y by SILAR method are shown in Figs. 8-16. Nyquist plots are depicted in Figs. 8 and 9.

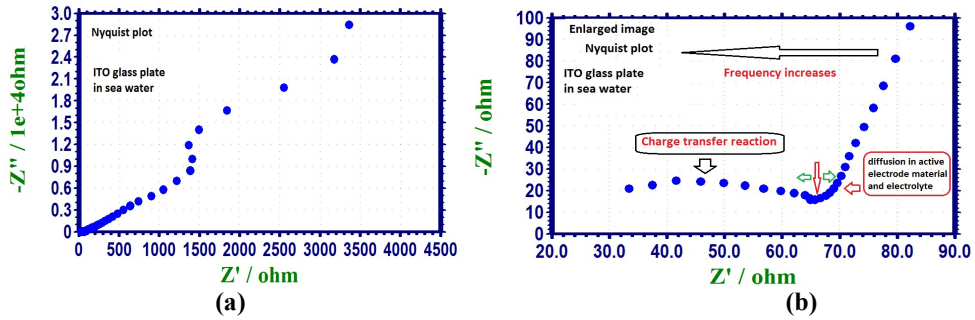

Figure 8: (a) Nyquist plot of ITO GP immersed in SW; **(b)(**enlarged image).

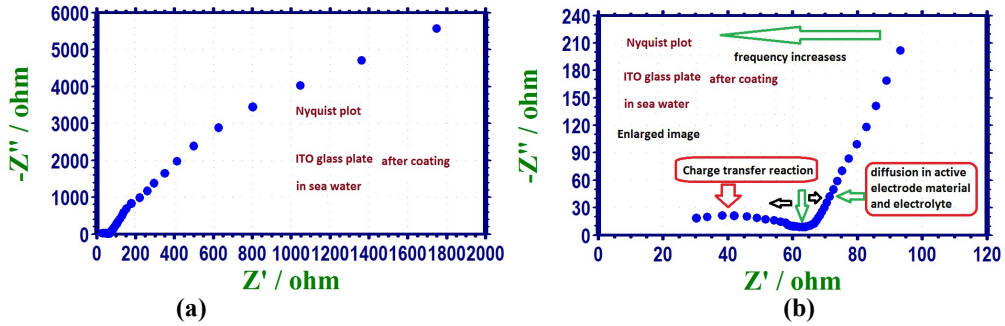

Figure 9: (a) Nyquist plot of ITO GP after coating in SW; **(b)** (enlarged image).

It is interesting to note that Figs. 8b and 9b depict diffusion controlled processes. The equivalent circuit diagram is shown in Scheme A.

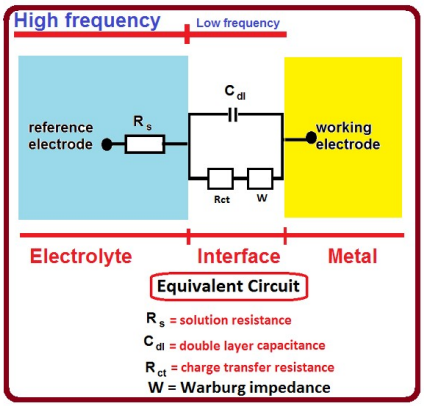

Scheme A: Equivalent circuit diagram for a diffusion controlled process.

Bode plots are shown in Figs. 10 and 11.

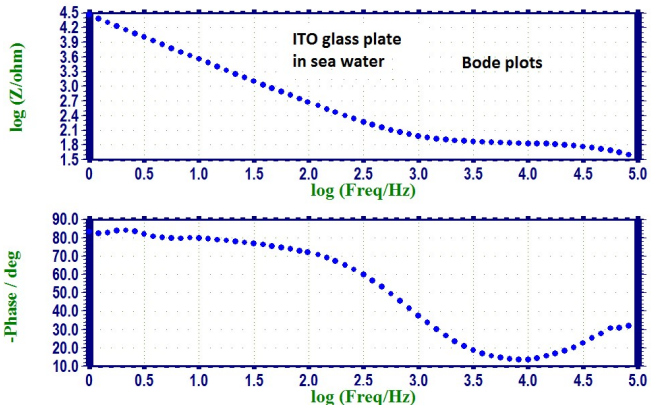

Figure 10: Bode plots of ITO GP immersed in SW.

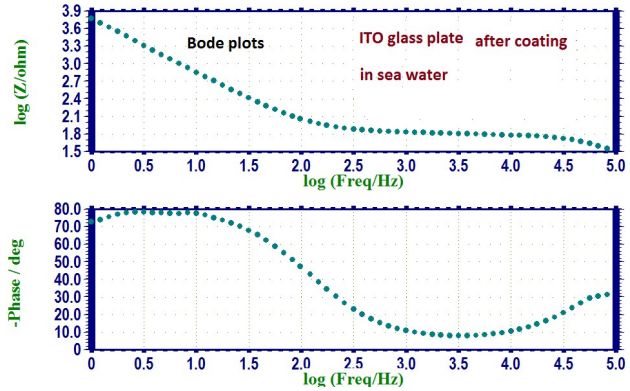

Figure 11: Bode plots of coated ITO GP in SW.

3D plots are shown in Figs. 12-15.

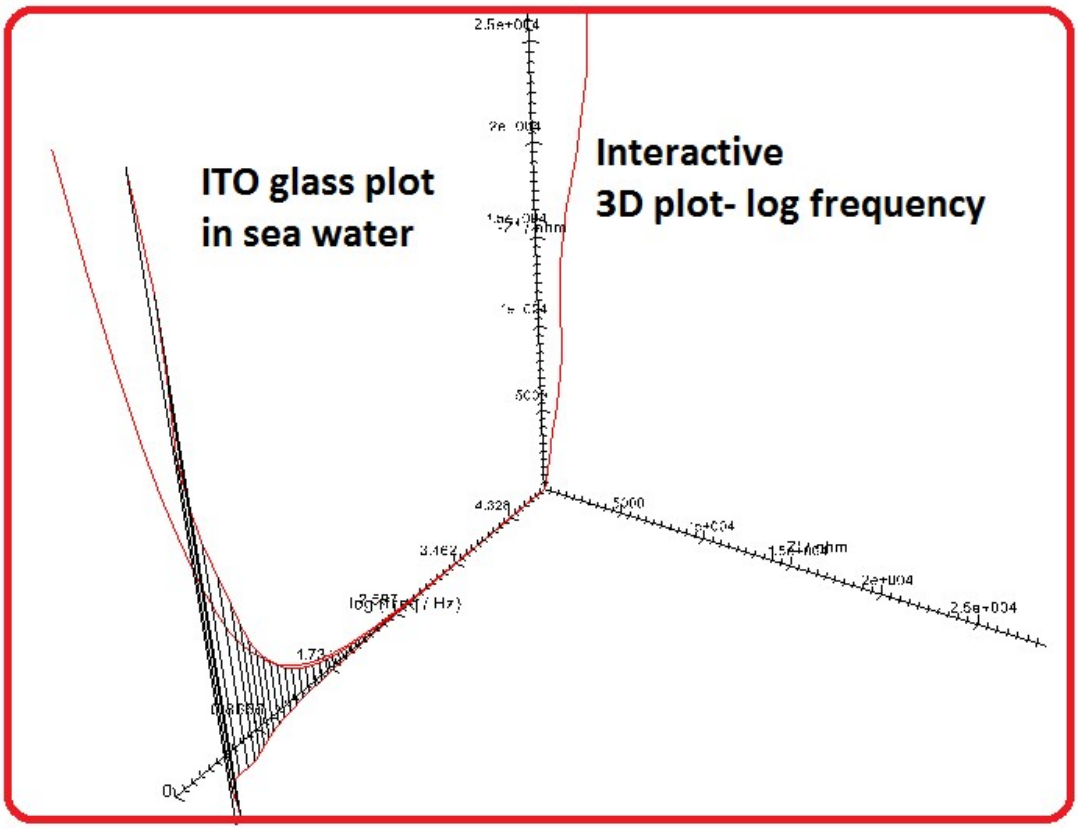

Figure 12: Interactive 3D plot-log frequency of ITO GP immersed in SW.

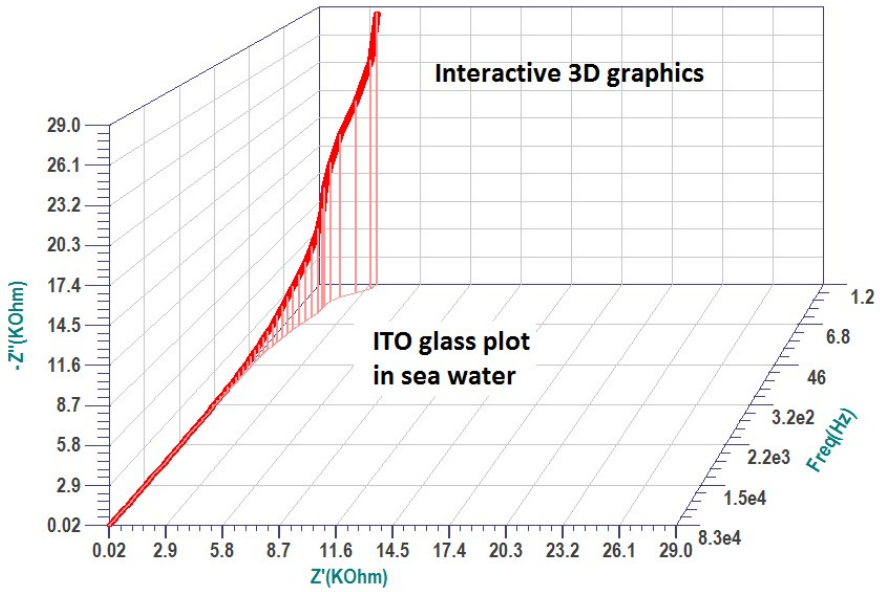

Figure 13: Interactive 3D graphics plot of ITO GP immersed in SW.

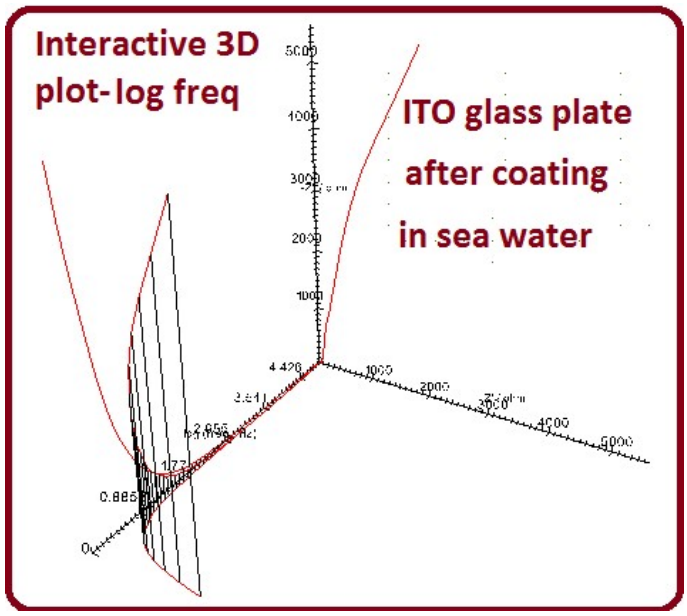

Figure 14: Interactive 3D plot-log frequency of coated ITO GP immersed in SW.

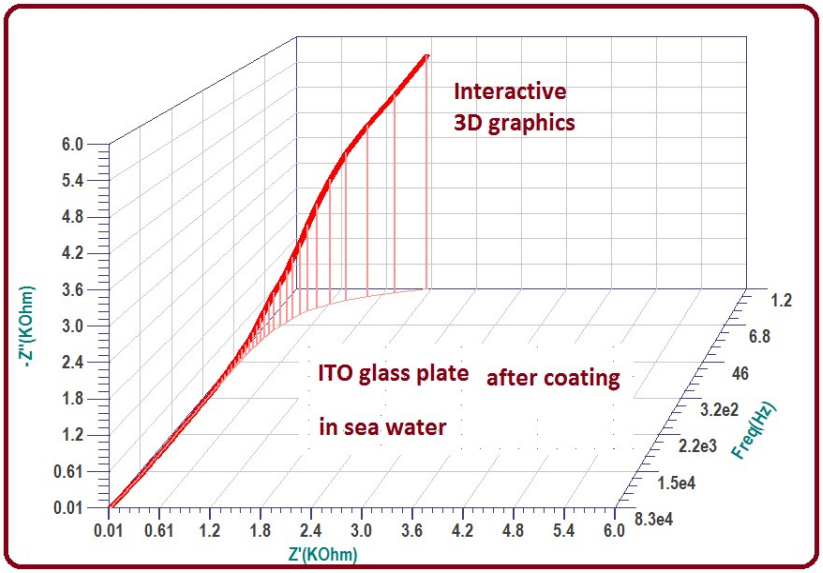

Figure 15: Interactive 3D graphics of coated ITO GP immersed in SW.

The parameters derived from AC impedance spectra, namely, R_{ct}, C_{dl}, impedance and phase angle are given in Table 2.

It was observed that, after coating, R_{ct} decreased from 3555 to 1750 Ohm/cm^2 and C_{dl} increased from 1.4214×10^{-9} to 2.8651×10^{-9} F/cm^2. Impedance and phase angle values decreased from 4.464 to 3.772° and from 30.74 to 29.12°, respectively. It was inferred that, after coating ITO GP with Ni_xS_y by SILAR method, the current flowing through it increased [22-30]. Such systems may find application in solar cells located in marine environments.

Table 2: AC impedance parameters of ITO GP immersed in SW before and after coating with Ni_xS_y by SILAR method.

System	R_{ct} Ohm/cm^2	C_{dl} F/cm^2	Impedance log (Z/ohm)	Phase angle
Uncoated GP in SW	3555	1.4214×10^{-9}	4.464	30.74
Ni_xS_y-coated GP in SW	1750	2.8651×10^{-9}	3.772	29.12

1/Sqrt (w) *vs.* Z"& Z'/ohm plots are shown in Fig. 16. Polarisation study and AC impedance spectra revealed that, after ITO GP coating with Ni_xS_y film, the current flowing through it increased. From Fig. 16, it was inferred that, in y-axis, the gap between the two extremes decreased after coating.

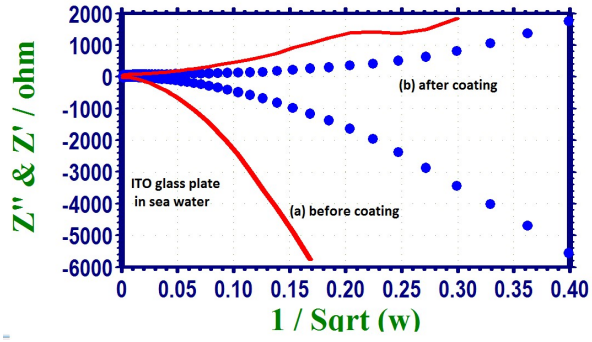

Figure 16: 1/Sqrt(w) *vs.* Z"and Z'/ohm plots.

Conclusion

A thin film of Ni_xS_y was deposited on ITO GP. This film was characterized by UV-vis reflectance spectroscopy and FTIR spectra. UV-vis reflectance revealed that E_g of Ni_xS_y film was 1.55 eV. After coating, E_g of ITO GP decreased from 1.88 to 1.55 eV. This indicates that the film functioned as semiconductor. UV-vis absorption study of the film indicates that absorbance took place at 322.00, 388.80 and 396.25 nm, with peak intensity of 1.229 (Au), 0.934 (Au) and 0.916 (Au), respectively.

FTIR spectra confirmed the formation of Ni_xS_y on ITO GP by SILAR method. Electrochemical studies, such as polarization technique and AC impedance spectra, revealed that the current flowing through ITO GP increased after Ni_xS_y coating by SILAR method. The findings of this study may be useful in solar panel systems employed in marine environments.

Authors' contribution

N. Karthika: coordinated of the present work. **B. Gomathi, A. L. Jewelcy, A. C. Jamuna, R. Jeyalakshmi, P. S. L. Kala**: prepared Ni_xS_y thin film on ITO GP by SILAR method; recorded electrochemical studies; recorded UV-vis and FTIR spectra. **M. Pushpa, N. Anitha**: conceptualization and validation; review and editing. **S. Rajendran**: writing, correspondence. All authors have read and agreed to the published version of the manuscript.

Acknowledgement
The authors are thankful to their managements for their help and support.

Abbreviations
AC: alternating current
Ag_2Se: silver selenide
AU: arbitrary unit
Bi_2S_3: bismuth sulfide
C_{dl}: double layer capacitance
E_{corr}: corrosion potential
E_g: band/energy gap
EIS: electrochemical impedance spectra
FTCD: flow-through chemical deposition
FTIR: Fourier transform infrared spectroscopy
GP: glass plate
I_{corr}: corrosion current density
ITO: indium tin oxide
LPR: linear polarization resistance
Ni_xS_y: nickel sulfide
RBS: Rutherford Backscattering Spectroscopy
R_{ct}: charge transfer resistance
SCE: saturated calomel electrode
SILAR: successive ionic layer adsorption and reaction
SW: sea water
TE: thermoelectric

Symbols definition
β_c: cathodic Tafel slope
β_a: anodic Tafel slope

References
1. Amudhavalli B, Mariappan R, Prasath M. Synthesis chemical methods for deposition of ZnO, CdO and CdZnO thin films to facilitate further research. J All Comp. 2022;925:166511. https://doi.org/10.1016/j.jallcom.2022.166511
2. Cruz MRA, Luévano-Hipólito E, Garza-Hernández R et al. MgO and Mg(OH)2 thin films prepared by the SILAR method and their CO2 photocatalytic performance. J Mater Sci. 2022;57(40):18739-18753. https://doi.org/10.1007/s10853-022-07837-x
3. Yücel E, Yücel Y. Deposition of PbS thin films using a continuous flow reactor: Comparison of the modified technique with conventional methods in the coating of PbS thin film on the substrate. J Ind Chem Soc. 2022;99(10):100706. https://doi.org/10.1016/j.jics.2022.100706
4. Jostar ST, Devadason S, Arputhavalli GJ et al. Physica Enhancement of opto-electrical properties in Co doped CdS–TiO_2nanocomposite thin film as photoanode for Semiconductor Sensitized Solar Cells (SSSCs). E: Low-Dimens Syst Nanostruc. 2022;142:115287. https://doi.org/10.1016/j.physe.2022.115287

5. Klochko N, Barbash V, Klepikova K et al. Flexible thermoelectric and photosensitive thin-film material based on nanostructured ZnO:In layer covered by nanocellulose. Mater Tod: Proceed. 2022;62:5819-5832. https://doi.org/10.1016/j.matpr.2022.03.500
6. Shivasharma TK, Bommineedi LK, Sankapal BR. Pseudo capacitive nano structured silver selenide thin film through room temperature chemical route: First approach towards super capacitive application. Inorg Chem Commun. 2022;135:109083. https://doi.org/10.1016/j.inoche.2021.109083
7. Roa S, Sandoval M, Suárez S. H_2O_2 as a strong catalyzer for the growth velocity of SILAR-deposited ZnO thin films. Chem Phys Lett. 2022;787:139233. https://doi.org/10.1016/j.cplett.2021.139233
8. Bouachri M, El Farri H, Beraich M et al. Influence of cycle numbers on optical parameters of nanostructured Bi2S3 thin films using SILAR method for solar cells light harvesting. Materialia. 2021;20:101242. https://doi.org/10.1016/j.mtla.2021.101242
9. Klochko NP, Klepikova KS, Khrypunova IV et al. Flexible thermoelectric module based on zinc oxide thin film grown via SILAR. Curr Appl Phys. 2021;21:21-133. https://doi.org/10.1016/j.cap.2020.10.012
10. Bahrawy AA, Ibrahim AA, El-Rabiei MM et al. Hierarchical porous nickel tin sulfide nanosheets as a binder free electrode for hybrid supercapacitor. J Ener Stor. 2023;73:109002. https://doi.org/10.1016/j.est.2023.109002
11. Vishnu NV, Jagannathan BS, Rajni KS. SILAR deposited Cu2MnSnS4 thin films for sustainable energy applications. Mater Lett. 2024;359:135875. https://doi.org/10.1016/j.matlet.2024.135875
12. Pawar DC, Malavekar DB, Lokhande AC. Facile synthesis of layered reduced graphene oxide/polyaniline (rGO/PANI) composite electrode for flexible asymmetric solid-state supercapacitor. J Ener Stor. 2024;79:110154. https://doi.org/10.1016/j.est.2023.110154
13. Satılmış H, Acar M, Aydın R et al. Cd-supported CuO-ZnO binary oxide thin films: Synthesis, microstructural, and optoelectronic properties. 2024;148:114851. https://doi.org/10.1016/j.optmat.2024.114851
14. Bronusiene A, Kleinauskas R, Ancutiene I. Facile Synthesis and Characterization of TiO_2/SnS Nanocomposites by Eco-Friendly Methods. Coatings. 2024;14(1):88. https://doi.org/10.3390/coatings14010088
15. Horoz B, Tuna Yıldırım S, Soltabayev B et al. Effect of SILAR cycle on gas sensing properties of In_2O_3 thin films for CO gas sensor. J Mater Sci. 2024;35(2):163. https://doi.org/10.1007/s10854-024-11970-5
16. Rajan K, Thangaraju D, Prakash N et al. Single Step Synthesis and Catalytic Activity of Structure controlled Nickel Sulfide Nanoparticles. Cryst Eng Comm. 2015;17(29):5431-5439. https://doi.org/10.1039/C5CE00742A
17. Rathod RL, Rajappa MR, Sajjan SK et al. Experimental and Theoretical Investigations of *Cordia Obliqua* Leaves Extract as an Environmentally Benign Inhibitor for Mild Steel Corrosion in a 1 M HCl Solution. Port Electrochim Acta. 2024;42(4):233-254. https://doi.org/10.4152/pea.2024420401

18. Khanna R, Kalia V, Kumar R et al. Synergistic experimental and computational approaches for evaluating pyrazole Schiff bases as corrosion inhibitor for mild steel in acidic medium. J Mol Struct. 2023;1297:136845. https://doi.org/10.1016/j.molstruc.2023.136845
19. Karamuzzzan WM, Shaifudin MS, Nasir NAM et al. Experimental, DFT and molecular dynamic simulation of *Andrographis paniculata* as corrosion inhibitor for mild steel in artificial seawater. Mater Chem Phys. 2024;312:128642. https://doi.org/10.1016/j.matchemphys.2023.128642
20. Yıldız R, Arslanhan S, Döner A et al. Corrosion behavior of mild steel in 1 M HCl with *Cyclotrichiumniveum* as a green inhibitor. Mater Chem Phys. 2023;312:128654. https://doi.org/10.1016/j.matchemphys.2023.128654.
21. Bedair MA, Abuelela AM, Melhi S et al. Highly effective inhibition of steel corrosion in 1.0 M HCl solution using a novel non-ionic surfactant with Coumarin moiety: Practical and computational studies. Mater Chem Phys. 2024;312:128644. https://doi.org/10.1016/j.matchemphys.2023.128644.
22. Shaaban MS, Shalabi K, Fouda A et al. New imidazolium-based ionic liquids for mitigating carbon steel corrosion in acidic condition. Zeitsch Physik Chem. 2023;237(3):211-241. https://doi.org/10.1515/zpch-2022-0155
23. Nilavan A, Jewelcy AL, Thomas AA et al. Corrosion resistance of mild steel immersed in simulated concrete pore solution in the presence of sodium potassium tartrate. Mater Prot. 2023;64(2):170-176. https://doi.org/10.5937/zasmat2302170N
24. Anita N, Joany RM, Dorothy R et al. Linear polarization resistance (LPR) technique for corrosion measurements. Electrochem Analyt Techn Sustain Corros Monit: Adv Chall Opport. 2023;59-80. https://doi.org/10.1016/B978-0-443-15783-7.00005-0
25. Nilavan A, Rajendran S. Inhibition of corrosion of L 80 alloy in sodium hydroxide solution (pH=12) by succinic acid. Mater Prot. 2023;64(1):78-85. https://doi.org/10.5937/zasmat2301078K
26. Sheit HMK, Mubarak MS, Benitta G. Anti-Corrosive Efficiency of Mild Steel in Sodium Chloride Solution Using 5-Acetyl-3-Phenyl-2, 6-Dipyridin-2-Yltetra-Hydropyrimidin-4(1H)-1 Compound as an Inhibitor. J Bio- Tribo-Corros. 2022;8(4):103. https://doi.org/10.1007/s40735-022-00703-y
27. Khatbi S, Gouale Y, Lamiri A et al. Electrochemical and Metallurgical Behavior of Lead-Silver Casting Alloys as Grids for Lead-Acid Batteries. Port Electrochim Acta. 2025;43(2):127-139. https://doi.org/10.4152/pea.202543020
28. Ugi BU, Boekom JE, Ashishie PB et al. Scopolamine Alkaloid as Novel Green Inhibitor of Malleable Fe Corrosion Studied by EIS, DFT, PDP and SEM Techniques. Port Electrochim Acta. 2025;43(1):23-35. https://doi.org/10.4152/pea.2025430103
29. Ompal SY, Reshu C, Ashu G. Synthesis of Green Inhibitor for Mild Steel Corrosion in a Sulphuric Acid Medium. Port Electrochim Acta. 2024;42(5):355-373. https://doi.org/10.4152/pea.2024420504
30. Minagalavar RL, Rathod MR, Rajappa SK et al. Experimental and Theoretical Investigations of *Cordia Obliqua* Leaves Extract as an Environmentally Benign Inhibitor for Mild Steel Corrosion in a 1 M HCl Solution. Port Electrochim Acta. 2024;42(4):233-254. https://doi.org/10.4152/pea.2024420401